Building and Environment 112 (2017) 177–189

Contents lists available at ScienceDirect

Building and Environment

journal homepage: www.elsevier.com/locate/buildenv

Evaluation of canopy-layer air and mean radiant temperature simulations by a microclimate model over a tropical residential neighbourhood

Matthias Roth*, Vanessa Huimin Lim

Department of Geography, National University of Singapore, 1 Arts Link, Kent Ridge, 117570, Singapore

ARTICLE INFO

Article history:
Received 20 July 2016
Received in revised form
27 October 2016
Accepted 12 November 2016
Available online 14 November 2016

Keywords:
ENVI-met
Microclimate modeling
Canopy-layer temperature
Mean radiant temperature
Urban climate
Singapore

ABSTRACT

The performance of a 3D urban microclimate model (ENVI-met Version 3.1) is evaluated with data collected during mostly clear and calm conditions in a compact low-rise residential neighbourhood of tropical Singapore. Observations are obtained from seven canopy-layer air temperature, T_a, sensors at 2 m above ground, including a fully equipped microclimate station measuring mean radiant temperature, *MRT*, at 1.1 m above ground. The model is capable of capturing the spatial variability across all stations during most of the eight simulation days. Spatially-averaged T_a predictions are closer to the observations during wet (based on five simulation days) compared to dry (three days) periods. Daytime model performance for *MRT* is variable but peak values are well predicted. Systematic errors dominate most simulations. The present model evaluation metrics are smaller than reported in similar work, which is likely due to the more accurate determination of model input variables using locally measured soil relative humidity and leaf area density profiles. A modification to how the model calculates *MRT* also helps to improve its daytime performance. Finally, the model is used to predict the effect of five temperature mitigation/planning strategies. The varying results highlight the micro- and bioclimatic complexities inherent in a heterogeneous urban system, with no one scenario providing consistent cooling throughout both day- and nighttime. Overall the present results suggest that ENVI-met is a useful planning tool for assessing T_a and daytime extremes in outdoor thermal comfort, but the model requires detailed local information for proper initialization and awareness of its limitations.

1. Introduction

Urbanization radically alters the physical environment from its natural state, and has inadvertent albeit important environmental consequences. The aerodynamic, thermal, radiative and hydrological processes characteristic of natural environments are changed through modifications of surface morphology, introduction of artificial surfaces, reduction in vegetation cover and emission of urban pollutants [1]. As a consequence cities experience elevated air temperatures and have a different thermal regime from that of surrounding rural, undeveloped areas [2]. Such elevated temperatures are clearly undesirable in cities in the humid tropics where the combination of high air temperature and humidity, intense solar radiation and low wind speed results in thermally stressful conditions throughout the year [3]. Some of the consequences of the additional urban warmth superimposed on already high mean air temperatures include a reduction in outdoor thermal comfort (OTC) with detrimental impacts on human health and mortality, or an increase in demands for air conditioning and hence energy usage. A global climate model with an embedded urban model further predicts that the tropics will experience the greatest increase in number of high-heat-stress nights under a global warming scenario [4]. Urban climate research should therefore assume a high priority in the humid tropics where rapid urban growth is occurring [5] and the improvement of OTC should be a key planning consideration [6].

Microclimate models are useful tools to predict climatic features of the urban environment and they provide an important means of assessing feedback relationships between urban modifications and the climate, and vice versa [7]. These models offer the flexibility of evaluating a wide range of urban configurations for a specific purpose or to answer explicit urban planning and design questions. If

* Corresponding author.
E-mail address: geomr@nus.edu.sg (M. Roth).

http://dx.doi.org/10.1016/j.buildenv.2016.11.026
0360-1323/

the models are accurate, they provide an alternative to time-consuming and costly field measurements, and are the only way to predict future climate conditions arising from planning interventions. The choice of the most appropriate model depends on the research question asked. Several models such as RayMan [8], SOLWEIG [9], SkyHelios [10] and ENVI-met [11] are capable of predicting biometeorologically relevant variables at very high spatial resolution. ENVI-met remains the most widely used model, perhaps because of its longer existence and relative ease in operation.

ENVI-met has been used to examine the urban microclimate or impacts of typical UHI mitigation strategies on air temperature and thermal comfort in mostly low-rise residential neighbourhoods. Studies have been conducted in humid (sub)tropical cities such as Colombo, Sri Lanka [12,13], Dhaka, Bangladesh [14], Shanghai, China [15], Hong Kong [16] or Putrajaya, Malaysia [17], and hot/dry cities such as Fez, Morocco [18,19], Melbourne, Australia [20], Phoenix, USA [21–25], Lecce and Rome, Italy [26,27]. The most recent version of ENVI-met has been extensively evaluated over sub-tropical Guangzhou, China [28] and was also tested in Rome [27].

An important, yet often neglected part of modeling is the proper initialization and evaluation of models [2]. Without proper evaluation to test the reliability of its output, the application of a model is questionable and it cannot be used as a trustworthy guide to policy formulation [29]. Although ENVI-met has been widely applied, its evaluation has not always been rigorous and until recently focussed primarily on canopy-layer air temperature (T_a). Some studies found that ENVI-met underestimates (overestimates) daytime (nighttime) T_a [12,21,22], others reported overestimation of daytime (or part thereof) T_a [15,24], and yet others have found underestimation of both day- and nighttime T_a [13,20]. Most research evaluates predictions for a single day or a few hours only [13,14,16,21,22], and only very few studies investigate the performance to assess the small-scale spatial variability the model is designed to predict [22,24,28]. With the exception of [24,28] most work also did not obtain site-specific initialization data (e.g. soil moisture and temperature) and instead used values from outside the modeling domain (e.g. from weather stations at nearby airports). In addition, there has been limited application of the model to hot and humid climates with only three studies carried out in Colombo, Dhaka and Putrajaya (see above). Furthermore, evaluations of other variables such as the biometeorologically relevant *MRT* are non-existent despite its use as an indicator of thermal comfort.

In order to address some of the existing research gaps, the first objective of the present study is to critically evaluate the accuracy of ENVI-met 3.1 in predicting the temporal dynamics of T_a and *MRT* during different seasons over a compact low-rise residential neighbourhood located in humid tropical Singapore. Since the model was initially developed for temperate climates, it cannot be assumed *a priori* that the default input parameters are applicable in the present context. The study area is therefore carefully represented in ENVI-met using selected site-specific input data from field measurements. Although an updated, improved ENVI-met Version 4 [30] has recently been released, the present research provides an assessment of past studies that have used the same version employed herein. Further, since some aspects of the model have not been updated in the new version (e.g. the soil model) any additional insight even from an older version will still be useful. The second objective is to estimate how T_a will be influenced by the implementation of common UHI mitigation strategies which include the modification of albedo, vegetation and building heights.

2. Methods

2.1. Study area

Singapore is a low-lying island city-state located between 1°09 N to 1°29 N, and 103°36 E to 104°25 E, just south of Peninsular Malaysia. Owing to its geographical proximity to the equator, Singapore has a tropical rainforest climate (Köppen classification, *Af*), which is characterized by uniformly high temperatures (annual mean: ~27 °C) and abundant annual rainfall (~2340 mm). Mean monthly rainfall peaks during the northeast (NE) monsoon period (>250 mm month^{-1}) between December to early March while the southwest (SW) monsoon period (June–September) typically experiences drier than average conditions (~150 mm month^{-1}). Wind speed measured 10 m above surface is generally low (1.3–2.8 m s^{-1}). During the remaining months of the year (i.e. inter-monsoon, IM, periods), surface winds are light with variable directions and possibly influenced by land and sea breezes. Synoptic weather conditions vary little across the island due to Singapore's small size and lack of topography, although isolated, small convective systems can result in localized rainfall. However, heterogeneity in the urban landscape (e.g. downtown central business district vs. residential neighbourhoods) gives rise to micro-scale and local differences in temperature and moisture regimes [6,31]. The combination of high T_a, relative humidity (*RH*) and low surface wind speeds has important consequences for thermal comfort in the tropics which is likely made worse by the UHI given Singapore's extensive urbanization [6,32].

The present study area is located in the low-density residential neighbourhood of Telok Kurau (TK) ~3 km north of Singapore's south-eastern coastline. A ~23 ha (548 × 428 m) area constitutes the model domain (Fig. 1) which is characterized by densely-placed low-rise buildings with mean (z_{mean}) ± 1 standard deviation, median (z_{median}) and maximum (z_{max}) building heights of 10.6 ± 4.7, 9.0 and 25.0 m, respectively. Buildings are a mixture of semi-detached houses (duplexes), terrace (row) houses and individual bungalows, interspersed with several taller (up to five storey high) condominiums. The compact low-rise area corresponds to Local Climate Zone (LCZ) 3 [33]. Although TK is not representative of the more common high-rise neighbourhoods in Singapore, it is undergoing rapid transformation where new condominium developments are replacing low-rise houses. Resident population density is ~7500 persons/km^2 and hence similar to the city-wide average.

The main street (Telok Kurau Road) traversing the study area has a SE–NW orientation and runs along the western edge of the model domain (Fig. 1). Secondary streets connected to the main street are orientated WSW-ENE. Tertiary streets perpendicular to the secondary streets are typically cul-de-sacs leading to residential homes and have similar orientations as the main street (NW-SE). Both main and secondary streets are lined with shade trees with heights (z_{tree}) ranging between 3.5 and 11.2 m. Individual houses usually have small gardens planted with turf grass, shrubs and small trees. There are several recreational grass fields with a combined size of ~1.2 ha in the study area. Slightly more than half (~1.1 ha) of an adjacent park (~1.8 ha) to the NE is also included in the model domain (Fig. 1). The study area is dominated by impervious surfaces, with buildings covering 39.8%, pavements 35% and roads 8.5% of the surface. Vegetation comprises 15.7% of the area where 7.6% and 8.1% are grass and trees, respectively. Other uses (water bodies and gravel) constitute only ~1%. The TK neighbourhood has recently been used in a number of urban flux studies which provide more detail on the site characteristics [34,35].

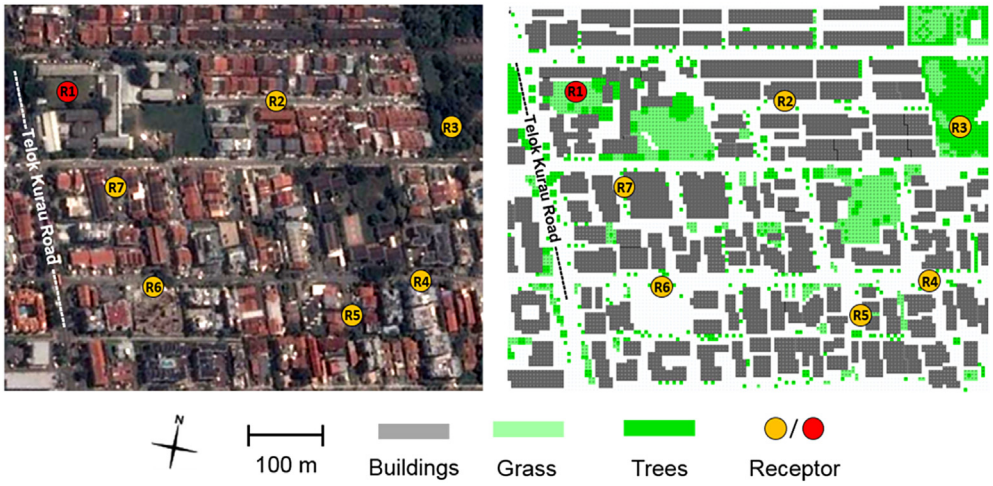

Fig. 1. (Left) Satellite view (Google Earth™) of Telok Kurau (TK) study area and (right) corresponding ENVI-met model area input file. The seven sensor/receptor locations are R1 (measuring air temperature, relative humidity, globe temperature, soil temperature and moisture, wind speed and direction at 1.1 m above surface; additional 2 m for air temperature) and R2 – R7 (air temperature and relative humidity at 2 m).

2.2. Microclimate measurements

Measurements were carried out at seven locations distributed across the model domain (Fig. 1), coinciding with the model "receptor" locations (see below). The main microclimate station was installed at R1 which is located in a semi-enclosed, grass-covered courtyard in the NW corner of the study area. Measurements included wind speed (u) and direction (θ) with a 034B wind set (Campbell Scientific Inc, Logan, Utah, USA), T_a and RH with a HMP45C (Vaisala, Helsinki, Finland), and globe temperature (T_g) with a globe thermometer at 1.1 m above the surface. An additional HMP45C sensor measured T_a and RH at 2 m above the surface. The height of the T_g observations coincides with the location of the human core and together with the wind speed at the same height was used to calculate MRT. The globe thermometer was constructed according to [36] by inserting a PT100 sensor (Omron E-52; Omron Industrial Automation, Kyoto, Japan) into a hollow 40 mm acrylic sphere that was painted flat grey (Nippon Pylox 45 Grey). MRT was calculated following [37]:

$$MRT = \left[(T_g + 273.15)^4 + \left(\frac{1.335 \cdot 10^8 u^{0.71}}{\varepsilon D^{0.4}} \right) (T_g - T_{a-1.1m}) \right]^{0.25} - 273.15 \quad (1)$$

where $1.335 \times 10^8\ u^{0.71}$ is the mean convection coefficient (MCC) (m s^{-1}) based on a calibration by Ref. [36],[1] ε and D are globe emissivity and diameter (m), respectively.

To evaluate the spatial variability predicted by the model, T_a and RH were measured at six additional sites (R2 – R7) using shielded, naturally aspirated sensors (HOBO ProV2, Onset Computer Corporation, Bourne, Massachusetts, USA) attached to lampposts at 2 m above the surface. A 7-day sensor comparison against the HMP45C was conducted at R1 after the observation period. Agreement was very good for T_a with differences of <0.2°C which is similar to the accuracy of the sensors involved. For RH the HOBOs recorded systematically higher values (by up to 14%) compared to the HMP45C. Respective adjustments were carried during post-processing. All meteorological data measured at R1 – R7 were sampled at 5 s and averaged over 30 min for comparison with the model output. The seven locations reflect the slight variations in morphological characteristics (e.g. sky view factor, SVF, green space) within the study area (Table 1), and when averaged provide more robust data representative of the entire domain compared to measurements at an individual location. Finally, rainfall and incoming short-wave solar radiation ($K\downarrow$) at 21 m above the surface were measured approximately 100 m southeast of R1 at an existing energy flux tower to select the clear days used in the present study.

2.3. Model setup, initialization and evaluation

ENVI-met is a three-dimensional (3D), grid-based computational fluid dynamics (CFD) model [11]. 3D wind flow is calculated using the incompressible, non-hydrostatic Navier-Stokes equations with the Boussinesq approximation. Turbulent exchange processes between vegetation, buildings and surfaces are resolved with a 1.5 order closure model based on k-epsilon equations [39]. Potential temperature and specific humidity are calculated using advection-diffusion equations and are modified by sources and sinks of heat and moisture within the model. Version 3.1 is used in the present study which, unlike Version 4, does not allow the specification of time-varying forcing data, or 1D profiles of atmospheric parameters [28].

The model has a user-selectable high spatial (0.5–10 m) and temporal (1–10 s) resolution, which makes it useful for assessing canopy-layer temperature and thermal comfort which can vary substantially over short distances and periods of time. The building layouts in the area input file (Fig. 1) are based on a GoogleEarth™ satellite image (captured March 2013) that has been cross-referenced with maps from OneMap [40]. Using a 4 × 4 × 4 m grid cell size the model environment comprises of a total of 137 × 107 x 15 cells, covering a horizontal area of 548 × 428 m extending 60 m above the surface with an equidistant vertical grid. The lowest grid cell is split vertically into five equally-spaced sections providing output at each section centre point to increase vertical model resolution and accuracy in calculating surface processes [11]. The two lowest model output levels are therefore at 1.2

[1] Tan et al. [38] calibrated grey globe thermometers in Singapore following [36] reporting an MCC of $3.42 \times 10^9\ u^{0.119}$ ms^{-1}. Using this value in Eq. (1), however, yields unrealistic results (MRT > 200 °C). This is likely because [38] used an incorrect definition of D (in mm rather than m) due to a typographical error in Ref. [36] (Thorsson, pers. comm.).

Table 1
Morphological characteristics and land cover of the seven measurement/receptor locations (R1 – R7). Sky view factor (SVF) at 2.0 m is calculated by ENVI-met. H/W – height-to-width ratio, z_h and z_{tree} – height of building and trees, respectively.

Location	SVF	H/W	Canyon orientation	Description
R1	0.84	0.28	ENE–WSW	Courtyard (~0.21 ha) with grass cover surrounded by mixture of taller (z_h = 9–13 m) to N and S and shorter (z_h = 4 m) to E and W buildings
R2	0.65	0.53	ENE–WSW	Street lined with terrace houses (z_h = 7–9 m)
R3	0.06	NA	NA	Recreational park mostly shaded by tree canopies (z_{tree} = 7–10 m)
R4	0.61	0.63	ENE–WSW	Asymmetric street canyon with taller condominiums (z_h = 11–18 m) on N side and combination of short houses and condominiums (z_h = 7–9 m and 17–20 m) on S side of street
R5	0.66	0.46	NNW–SSE	Cul-de-sac with bungalows (z_h = 7–14 m) on both sides of street
R6	0.79	0.21	ENE–WSW	Secondary street with terrace houses (z_h = 9–14 m) on N side; small condominium (z_h = ~11 m) and empty lot covered with gravel (~0.21 ha) on S side
R7	0.66	0.58	NNW–SSE	Cul-de-sac with short terrace houses (z_h = 7 m) on both sides of street

and 2 m above the surface and coincide with the observation heights. A smaller horizontal resolution of 2 × 2 × 2 m was tested but resulted in numerical instabilities, while a 3 × 3 × 3 m grid took ~7 days to run without significant differences in results compared to the 4 × 4 × 4 m grid. Similarly, a recent and possibly the only study investigating grid size sensitivity suggests minimal deviations in results when varying horizontal resolution between 1 × 1 and 3 × 3 m [27]. The present grid cell size represents a compromise between size of model domain, resolution and computation time. Four equidistant nesting grids (distance to the outermost grid boundary is 56 m) were used to reduce edge effects at the main domain boundary and improve numerical stability.

The model is run for 30 h starting at 0400 h LAT (= UTC + 8 h), with the first 6 h used as spin-up time for the model to achieve numerical stability. Dynamic time steps are used to ensure numerical stability at high solar elevation angles (γ), viz. 5 s during early mornings and evenings ($\gamma < 40°$), 2 s during mid-mornings and afternoons ($40° < \gamma < 50°$) and 1 s close to midday ($\gamma > 50°$). Simulations from 1000 h on the first until 0930 h on the next day are used for comparison against observations. The meteorological input data reflect average conditions during the duration of the simulation (Bruse, pers. comm.). Hence, T_a and *RH* are both spatially (across the domain) and temporally (over 30 h) averaged, and other input data measured at one location only (e.g. soil data for each layer or wind speed) are temporally averaged.

Since ENVI-met was developed for temperate climates, model default input parameters (e.g. for building parameters, vegetation, soil) are not necessarily applicable to the present study area. Site-specific information is therefore used. Heat transmittance values for building walls (U_w) and roofs (U_r) were obtained from an existing Building and Construction Authority of Singapore database [41] as 1.94 and 1.5 W m^{-2} K^{-1}, respectively. Default albedo values for roof (α_r) and walls (α_w) are 0.3 and 0.2, respectively, which is higher than the average albedo (~0.16) of the study area measured at the top of a nearby flux tower [35]. An area specific $\alpha_r = 0.16$ was subsequently adopted, while a higher $\alpha_w = 0.25$ was chosen to reflect the lighter colour of walls, similar to recommendations in Ref. [42].

A local vegetation database was constructed to reproduce the characteristics of trees. Common tree species were classified by height as short (ST) = <5.0, medium (MT) = 5.0–7.0 and tall (TT) = >7.0 m, respectively. Normalized leaf area density (LAD) profiles were calculated for each group (Fig. 2). LAD was determined according to [43] using leaf area index (LAI) data from a National Parks Board of Singapore database [44]. The local vegetation database was modified to reflect the root area distribution (RAD) of tropical evergreen trees according to [45] using a global database [46] (Fig. 2). The main and secondary streets are typically lined with both tall shade trees with wide canopies (e.g. *Samanea saman* and *Swietenia macrophylla*) and small trees (e.g. *Xanthostemon chrysanthus*). The park in the NE corner of the model domain comprises a mixture of grass, short (e.g. *Plumeria ruberia*), medium (e.g. *Bauhinia purpurea*) and tall trees such as the yellow flame tree (*Peltophorum pterocarpum*). Individual backyards are usually planted with short and medium high trees.

The model requires average soil temperature (T_s) and relative soil humidity (*RSH*) at three layers (upper at 0–20, middle 20–50 and lower >50 cm depth, respectively). T_s (at 0.08, 0.35 and 0.65 m depth) and volumetric water content (θ) (at 0.08 and 0.65 m depth) were measured using TCAV and CS615/CS650 sensors, respectively (Campbell Scientific Inc, Logan, Utah, USA) at R1. *RSH* was derived as:

$$RSH = \left(\theta/\theta_{fc}\right)100\% \quad (2)$$

where θ_{fc} is volumetric water content at field capacity (Bruse, pers. comm.). Since θ was not measured in the middle layer, soil *RSH* here was interpolated from measurements in the upper and lower layers. Given the complexity of these measurements, they were only carried out at one location and the soil profile comprising loam (upper layer), clay (middle) and sand (lower) was assumed to repeat itself across the study area. Additional model input parameters such as wind speed at 10 m (u_{10}), specific humidity at 2500 m (q) and cloud cover were obtained from the Meteorological Service Singapore weather station located ~9 km to the east of the study area at Changi Airport (ICAO: WSSS). Given steady wind patterns associated with the monsoonal flow and absence of any topography, measurements from this location are assumed be representative for much of Singapore.

ENVI-met offers the option of using "receptors" to record the temporal evolution of output parameters at selected grid cells, and seven of these corresponding to locations R1 – R7 were placed in the model domain to facilitate comparisons between observations and simulations (Fig. 1). Model performance is evaluated using correlation and difference measures. While correlation measures such as the square of the Pearson product-moment correlation coefficient (r^2) determine the strength of relationships between variables, they do not inform about model accuracy. Here, accuracy is defined as the degree to which model-predicted (P) values approach the magnitudes of the observed (O) values [47]. Difference measures such as the root mean square error (RMSE) and its systematic ($RMSE_s$) and unsystematic ($RMSE_u$) components are more appropriate tests of model accuracy as they describe the magnitude of differences between P and O. $RMSE_s$ indicates errors resulting from flaws in model design or systematic errors in field observations and model initialization values. If RMSE is mostly composed of $RMSE_u$, on the other hand, the model is likely performing at its maximum possible accuracy [48]. Model

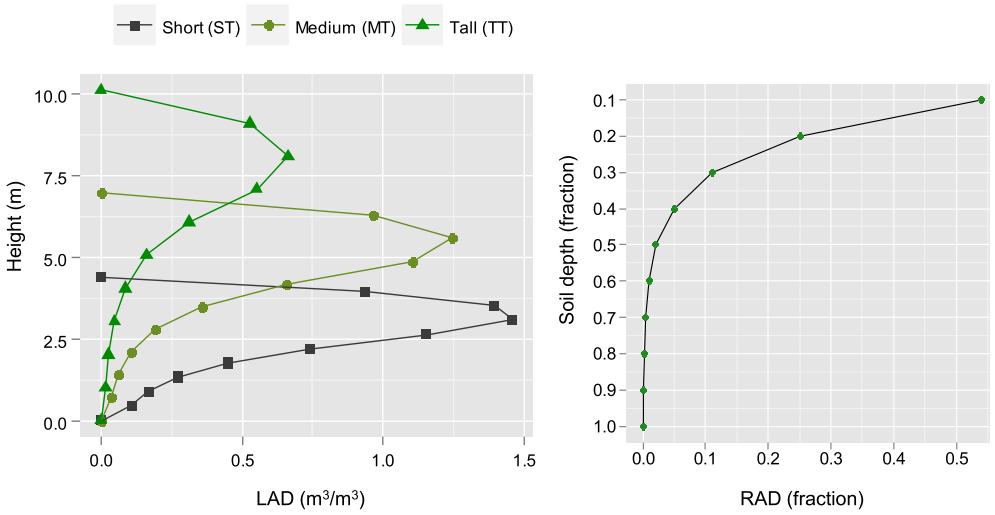

Fig. 2. Vegetation database values used in ENVI-met. (Left) vertical leaf area density (LAD) profile as a function of tree height for three height categories (ST, MT and TT); LAD is calculated according to [43] with leaf area index (LAI) data from a National Parks Board of Singapore database [44]. (Right) normalized root area distribution (RAD) profile calculated according to [45] with input data for tropical evergreen forests from Ref. [46].

performance is further evaluated using the dimensionless index of agreement (d), which measures the degree to which the model is error-free (ranges between 0.0 and 1.0).

2.4. Selection of simulation days

Observations were conducted between September 2012 – February 2013 and June – September 2013. Eight days (SIM1 – SIM8) were eventually selected for the simulations representing the IM (Sep–Nov 2012), NE (Dec–Feb 2013) and SW monsoon (Jun–Aug 2013) periods, respectively (Table 2). Since ENVI-met 3.1 cannot account for dynamic changes in cloud cover and rainfall, clear days were chosen for analysis. Days which maximize $K\downarrow$ and T_a further offer the opportunity to investigate periods with potential for high heat stress and therefore unpleasant OTC conditions. Completely clear and cloudless days, however, are rare in humid tropical locations and light cloud cover was present during most days. Daily total $K\downarrow$ ranged from 5400 to 6452 Wh m^{-2}. SIM1 – SIM3 represent the IM monsoon period and are characterized by low u_{10m} (<2.0 m s^{-1}) as well as drier and warmer soil conditions (Table 2). SIM4 – SIM5 during the NE monsoon period display higher u_{10m} (3.3–3.7 m s^{-1}) and *RSH* soil moisture due to increased rainfall. SIM6 – SIM8 reflect the SW monsoon period, with slightly higher average T_a than during the other seasons. *RSH* is particularly high during SIM6 and SIM8 (>90% in top layer) due to heavy rain preceding the two days on 18 and 27 July 2013, respectively. The soil characteristic, however, display considerable variability within one period. For example, the last rain event prior to SIM5 is 10 days earlier (24 October 2013) reducing *RSH* to levels comparable to those observed for SIM1 – SIM3.

3. Results

3.1. Evaluation of T_a simulations

To evaluate the model, the domain average calculated as the

Table 2
ENVI-met input parameters for meteorology, soil and building characteristics for eight simulation days (SIM) across three seasons. T_a – air temperature, *RH* – relative humidity (both at 2 m above ground), u_{10} – wind speed at 10 m, Θ_{10} – wind direction at 10 m, q_{2500} – specific humidity at 2500 m, T_s – soil temperature, *RSH* – relative soil humidity.

Input data	SIM							
	Inter-monsoon			NE-monsoon		SW-monsoon		
	1	2	3	4	5	6	7	8
Start of simulation	1 Oct 2012	8 Oct 2012	15 Oct 2012	29 Jan 2013	2 Feb 2013	21 Jul 2013	24 Jul 2013	28 Jul 2013
Meteorological data								
T_a at 2 m (°C)	29.7	29.8	28.8	28.9	29.0	29.5	30.0	29.2
RH at 2 m (%)	79.0	77.0	82.0	78.0	67	80.2	81.0	81.8
u_{10} (m s^{-1})	1.8	1.8	1.8	3.3	3.7	1.8	2.5	2.4
Θ_{10} (degrees from N)	225	220	0	45	45	200	180	180
q_{2500} (g kg^{-1})	7.0	9.6	10.2	6.8	7.0	6.0	9.2	8.0
Cloud cover (octas)	2	2	2	1	2	3	2	1
Soil data								
T_s (°C)/*RSH*[a] (%): upper layer (0–20 cm)	30.6/59.0	30.5/56.0	30.3/57.5	27.9/75.0	28.5/60.0	29.2/94.0	30.6/72.9	29.5/97.9
T_s (°C)/*RSH*[a] (%): middle layer (20–50 cm)	30.6/47.0	30.2/39.0	30.1/39.4	27.7/65.0	28.2/49.5	29.8/61.0	30.3/55.6	29.3/78.2
T_s (°C)/*RSH*[a] (%): lower layer (>50 cm)	30.4/33.8	30.2/22.0	30.1/19.3	27.8/40.0	28.2/39.5	29.7/29.0	30.1/36.4	29.5/56.3
Building inputs[b]								
Wall/roof albedo	0.25/0.16							
Wall/roof U-value (W m^{-2} K^{-1})	1.94/1.50							

[a] *RSH* is derived from volumetric water content which is a function of soil field capacity (Bruse, pers. comm.).
[b] Source: [41].

average from the individual sensors is compared to the average of the modelled data at the respective receptor locations. Since the sensor measuring T_a at 2 m at R1 was not installed until November 2012, the average for SIM1 – SIM3 consists of locations R2 – R7 only. To ensure that spatial averages based on six sensors (AVG6) are not significantly different from those derived using all seven sensors (AVG7), an independent-samples *t*-test was conducted to compare 240 pairs of AVG6 and AVG7 data from SIM4 – SIM8. No significant difference between AVG6 and AVG7 ($t[478] = 0.139$, $p = 0.89$) was observed and the maximum difference found between 240 pairs was 0.08 °C, which is well below the accuracy of the sensors (HMP45C: ±0.2–0.3 °C; HOBO: ±0.21 °C). Further statistical tests showed that averages derived from all individual grid cells were not significantly different ($p > 0.71$) from the domain averages. Hence the receptor averages are considered representative of the entire model domain.

The model is capable of simulating the main features of the diurnal variability of observed T_a, which follows the expected behaviour with relatively small diurnal amplitudes and little intra-seasonal variability in absolute magnitudes given the uniform climate context (Fig. 3). Differences between predicted and observed daytime T_a maxima are <0.6 °C with the exceptions of SIM2 and SIM5, which show larger over- and underprediction, respectively. The timing of the model peak is within ±2 h of the observed peak in the early afternoon (1230–1500 h). Minimum T_a is measured before or around sunrise (0400–0630 h) and is overpredicted in 5 of 8 cases (up to 2 °C in the case of SIM1). Modelled minimum T_a is delayed by 1–2 h and occurs just after sunrise (0630–0700 h). As a consequence of overpredicting minimum T_a the model diurnal ranges are generally smaller (4.7–5.8 °C) compared to the observations (4.9–6.9 °C). Similar results using ENVI-met have been reported in other studies as well [13].

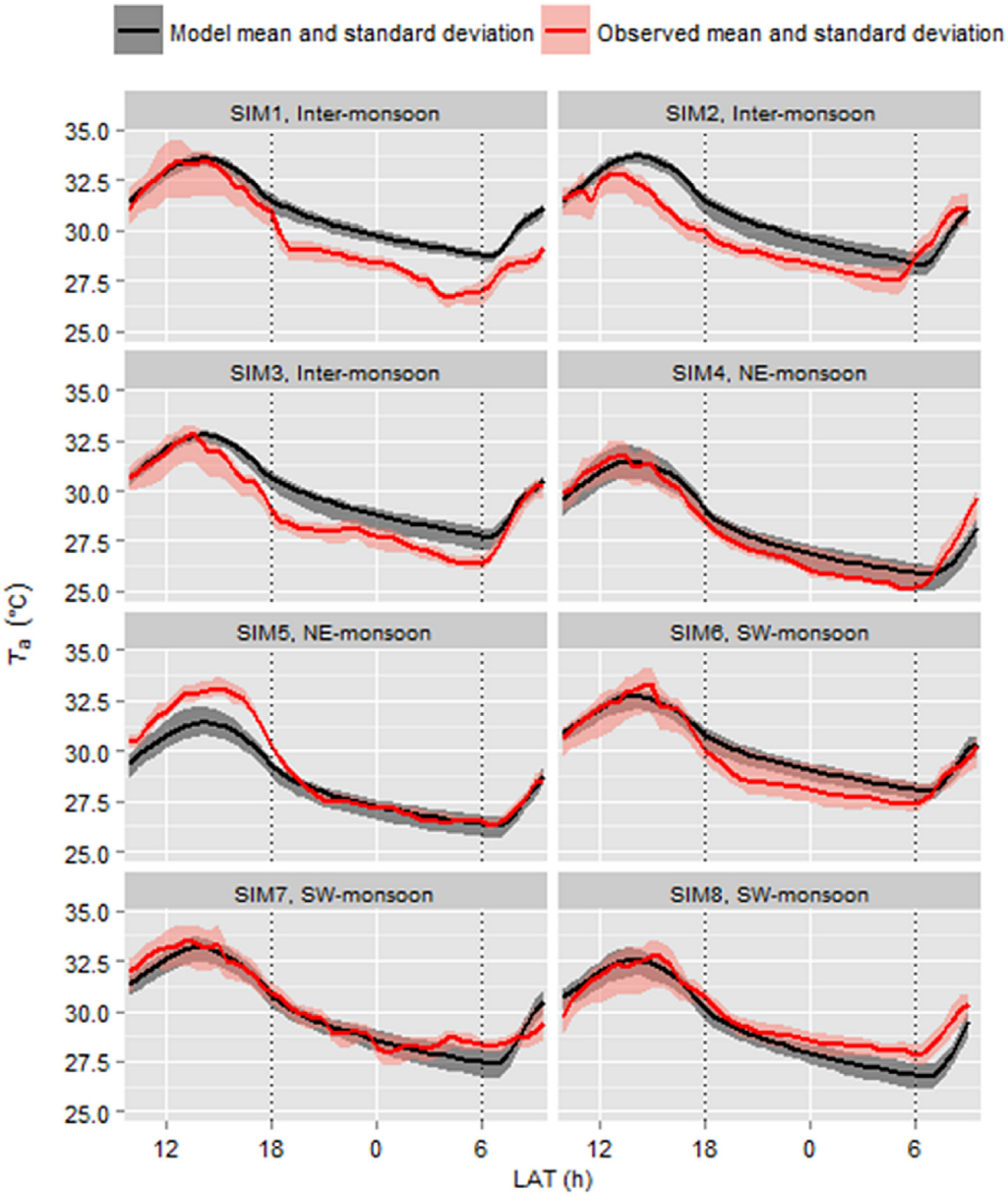

Fig. 3. Comparison between observed (red line) and simulated by ENVI-met (black line) diurnal variability of domain average 2-m air temperature (T_a) for eight days (SIM1 – SIM8) during three seasons. Red and grey shaded areas are ±1 standard deviation. Vertical dotted lines indicate time of sunset and sunrise, respectively. (For interpretation of the references to colour in this figure legend, the reader is referred to the web version of this article.)

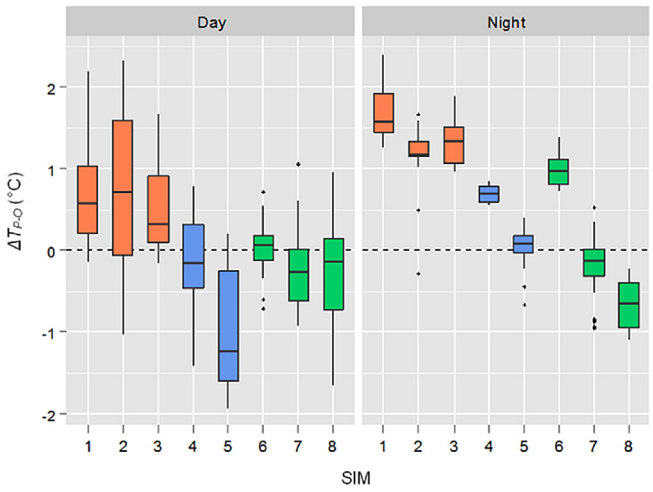

Fig. 4. Box plots showing differences between simulated by ENVI-met and observed domain average 2-m air temperature ($\Delta T_{P\text{-}O}$) for (left) daytime (0630–1800 h) and (right) nighttime (1830–0600 h) for eight days (SIM1 – SIM8) during three seasons. Orange – inter-monsoon, blue – NE monsoon, green – SW monsoon period; horizontal line, bottom and top in each box are median, 25th and 75th percentile, respectively, vertical lines extend between maximum and minimum values, black symbols are outliers. (For interpretation of the references to colour in this figure legend, the reader is referred to the web version of this article.)

The ability of ENVI-met to predict the diurnal dynamics of T_a depends to some extent on the season. The model performs poorly for all three simulations during the drier inter-monsoon period (SIM1 – SIM3) when both, day- and nighttime temperatures are overpredicted (Figs. 3 and 4). Good agreement is only observed during the morning hours until around noon, whereas afternoon T_a is overpredicted by up to 3 °C in the case of SIM1. The reverse is true for the wetter NE (SIM4 – SIM5) and SW monsoon (SIM6 – SIM8) periods when model agreement is better during day- compared to nighttime, with the exception of SIM5. The best agreement across the full day is found for SIM7 where average day- and nighttime model underestimation is <0.25 °C (Fig. 4).

The respective over- and underestimations of model domain-averages for individual simulation days are also reflected in the results for individual locations. There is no bias within the modeling domain and the model is able to capture the spatial variability of T_a (Fig. 5). Similar to the spatially-averaged T_a, all individual locations show large overestimation during the dry period (SIM1 – SIM3). The relative trend in daily median values is primarily due to daytime differences given that the spatial variation at night is much less (not shown). In terms of spatial differentiation, the daytime peak T_a is usually observed at R6 and in the case of the model at R6, R7 and R4. The high temperatures measured at R6 are plausible given its location next to an open construction site with little vegetation nearby (Table 1). The daytime T_a minimum is always measured and modelled at R3, reflecting the shaded nature of this park location. Observed daytime peak differences between the two stations measuring maximum and minimum T_a are between 1 and 2.5 °C with no dependence on season, and 0.8 and 1.8 °C based on modelled values where the lowest differences occur during the dry days (not shown). Observed nighttime minimum T_a is generally highest at R6 and lowest at R3 with differences of <1.5 °C. Although the model predicts similar T_a differences across stations, R3 only produces the lowest values in five simulations.

The daily model performance metrics for spatially averaged T_a confirm the above mostly qualitative analysis which shows better model performance during wet as opposed to dry conditions. SIM1 – SIM3 exhibit larger RMSE/MBE values (1.11–1.41°C/0.93–1.20 °C) due to large model overestimation, primarily at night, while smaller values (0.52–0.89°C/–0.51–0.52 °C) are obtained for SIM4 – SIM8 (Table 3). Systematic errors dominate with the exception of SIM4 and 7. Both, r^2 and d values are relatively high across the eight simulations ranging between 0.77–0.98 and 0.87–0.98, respectively. Despite the fact that SIM1 and SIM3 have r^2 values which are as high as those of other simulations, their d values are lower (0.88–0.91), demonstrating that high r^2 values do not necessarily indicate good model performance.

3.2. Evaluation of MRT simulations

MRT, only measured at R1, varies strongly between day- and nighttime. (Fig. 6). The daytime fluctuations in the observations (up to 15 °C) are due to sudden but brief changes in $K\downarrow$ which is highly correlated with *MRT* ($r = 0.95$; not shown). Despite taking care to select days that were as cloud free as possible, local, short-lived clouds due to small-scale convection can result in a temporary reduction of $K\downarrow$. Nighttime values on the other hand vary within a narrow range (23.6–25.9 °C). The model simulates these distinctive diurnal patterns with two important exceptions. First, the model predicts two daytime peaks (between 0900 and 1000 and at 1500 h, respectively) resulting in a characteristic double-humped shape with a minimum around 1200 h. This midday drop ranges between 2.7 and 6.4 °C across SIM1 – SIM8. Second, modelled nighttime *MRT* is systematically lower (ranging between 15.9 and 21.4 °C) and unlike the observations slowly declines throughout the night.

Although modelled *MRT* peaks at different times compared to the observations, ENVI-met appears to predict the maximum magnitude well, with differences of less than ±2.00 °C. The exception is SIM4 when the model underpredicts peak observations by 15 °C. Because of the underprediction of nighttime *MRT* the model tends to overestimate the diurnal range (by up to 7.6 °C). Separate performance metrics are therefore calculated for daytime and nighttime *MRT* (Table 3). RMSE/MBE range during daytime is larger (6.44 to 14.07°C/(–6.99 to 5.71 °C) than at night (4.21 to 9.18°C/–9.08 to –4.22 °C) as a result of the difference in peak behaviour discussed above. Unsystematic errors dominate during the day while systematic errors are larger at night. Despite large RMSE magnitudes, daytime d (0.77–0.96) and r^2 (0.59–0.80) values are relatively high. The large nighttime $RMSE_s$ together with the generally low d (0.11–0.65) and r^2 (0.00–0.51) values indicate that the model does not perform well at night but could be improved.

4. Discussion

4.1. Model performance for T_a

The present results show similarities, but also differences, to those obtained from similar studies carried out in other cities which exhibit a diversity of error patterns. The daytime (nighttime) underestimation (overestimation) of T_a found in SIM1 – SIM3, for example, was also observed over a heavily built-up site with little vegetation during a hot and humid 24 h period in Colombo, Sri Lanka [12] and during a 24 h period over a university campus site in hot and arid Phoenix, USA [21]. Other studies found that ENVI-met tends to overestimate daytime T_a, for example in two high-rise residential areas during a hot and humid 8 h summer period in Shanghai, China [15], and over three residential neighbourhoods with varying morphological characteristics during typical summertime conditions in Phoenix, USA [24]. On the other hand, [20] observed that ENVI-met tends to underestimate both day- and nighttime temperatures over a medium-density residential neighbourhood in Melbourne, Australia.

The fact that the systematic errors are generally larger than the

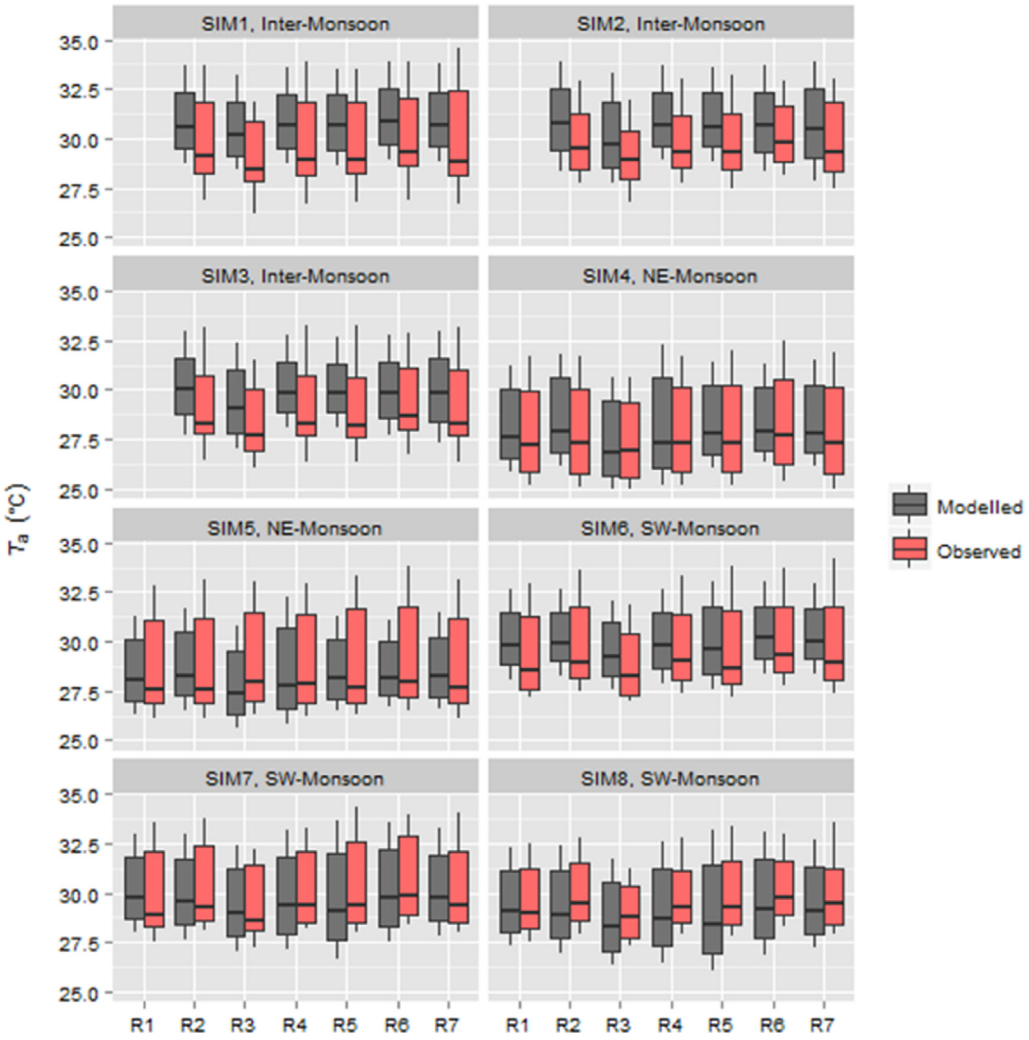

Fig. 5. Box plots showing observed (red) and simulated by ENVI-met (grey) diurnal range of 2-m air temperature (T_a) for eight days (SIM1 – SIM8) during three seasons. Horizontal line, bottom and top in each box are median, 25th and 75th percentile, respectively, vertical lines extend between maximum and minimum values excluding outliers. (For interpretation of the references to colour in this figure legend, the reader is referred to the web version of this article.)

unsystematic ones (Table 3) suggests that better model design or model initialization could improve agreement with observations. Most of the abovementioned studies ascribe nighttime model errors to the lack of building heat storage in ENVI-met 3.1 [12,21,22]. Lack of building heat storage likely also contributes to the current results. However, given that buildings occupy only 40.5% of the model area, sensible heat release from heat storage in non-built surfaces may also be important. The worse performance of the model during dry conditions further suggests that soil parameters play an important role. *RSH* (particularly in the uppermost soil layer) and daily RMSE during SIM1 – SIM3 are clearly lower (56.0–59.0%) and larger (1.11–1.41), respectively compared to SIM4 – SIM8 (60.0–97.9% and 0.52–0.89) (Tables 2 and 3). Similarly, the relatively drier SIM5 has the worst RMSE of the NE and SW monsoon simulations.

Only one other study has examined the influence of soil *RSH* [20] in ENVI-met 3.1. The results from a residential neighbourhood in Melbourne, Australia suggested that during dry conditions, when the model needs to be initialized with low soil *RSH* values (near wilting point), surface energy balance fluxes were wrongly partitioned with the consequence that the model overpredicting the Bowen ratio (ratio of sensible to latent heat flux) by more than a factor of two. d'Argent [20] ascribed this to constraints in the soil hydraulic model where vertical moisture transfers are limited, resulting in the topmost layer drying out too quickly. This in turn results in ENVI-met preferentially partitioning more energy into the sensible rather than latent heat, which leads to an overestimation of T_a. A sensitivity study was conducted using SIM1 to determine the relative importance of the initialization values by varying *RSH* and T_s in all three layers in steps of 10% and 1 °C, respectively, while holding all other input parameters constant. As expected, ENVI-met displays a particular sensitivity to dry soil conditions, where mean T_a increases by a larger amount (0.64–1.82 °C) when soil *RSH* is reduced by 10–30%, when compared to a similar increase which reduces T_a by a relatively smaller amount (0.21–0.23 °C) (Table 4). Sensitivity to T_s is less and T_a only changes between −0.37 and +0.5 °C when varying T_s by −3 and 3 °C, respectively. These results support the hypothesis that initial soil wetness is an important parameter that affects T_a, and could disproportionately influence model results when conditions become too dry.

Table 3
Difference measures of simulated by ENVI-met and observed domain average daily 2-m air temperature (T_a) and 1.1-m mean radiant temperature (MRT) for daytime (0630–1800 h) and nighttime (1830–0600 h), respectively at R1 for eight days (SIM1 – SIM8). RMSE – root-mean-squared error, $RMSE_s$ – systematic RMSE, $RMSE_u$ – unsystematic RMSE, MBE – mean bias error, MAE – mean average error, r^2 – coefficient of determination (dimensionless) and d – index of agreement (dimensionless).

	Difference measure						
	RMSE (°C)	$RMSE_s$ (°C)	$RMSE_u$ (°C)	MBE (°C)	MAE (°C)	d	r^2
Daily T_a							
SIM1	1.41	1.37	0.33	1.20	1.21	0.88	0.96
SIM2	1.27	0.97	0.83	0.96	1.15	0.87	0.77
SIM3	1.11	1.01	0.45	0.93	0.94	0.91	0.93
SIM4	0.66	0.43	0.5	0.27	0.60	0.97	0.93
SIM5	0.89	0.86	0.22	−0.5	0.61	0.95	0.98
SIM6	0.75	0.67	0.35	0.52	0.62	0.95	0.95
SIM7	0.52	0.2	0.47	−0.20	0.40	0.98	0.94
SIM8	0.75	0.61	0.43	−0.51	0.62	0.96	0.95
Daytime *MRT*							
SIM1	13.9	8.32	11.2	5.71	10.8	0.77	0.80
SIM2	9.53	3.25	8.96	2.39	8.08	0.88	0.62
SIM3	10.1	4.45	9.10	4.21	8.06	0.93	0.61
SIM4	14.1	9.56	10.3	−6.99	12.7	0.96	0.59
SIM5	9.95	3.8	9.19	−1.85	8.29	0.95	0.64
SIM6	6.56	1.46	6.34	1.16	5.14	0.93	0.80
SIM7	6.44	1.45	6.28	1.37	5.01	0.93	0.80
SIM8	6.69	2.43	6.24	1.95	5.73	0.94	0.80
Nighttime *MRT*							
SIM1	5.09	4.99	1.02	−4.99	4.99	0.33	0.08
SIM2	4.51	4.38	1.06	−4.38	4.38	0.11	0.14
SIM3	4.29	4.22	0.74	−4.22	4.22	0.17	0.51
SIM4	9.18	9.17	0.37	−9.08	9.08	0.86	0.83
SIM5	6.56	6.5	0.85	−6.47	6.47	0.65	0.03
SIM6	5.02	4.96	0.79	−4.96	4.96	0.35	0.34
SIM7	5.17	5.12	0.78	−5.11	5.11	0.38	0.33
SIM8	6.53	6.46	0.95	−6.45	6.45	0.58	0.00

4.2. Model performance for MRT

A number of reasons are suggested to explain the differences observed between predicted and observed *MRT*, some are specific to the present study and others are of more fundamental nature. In terms of measurements, *MRT* is estimated from T_g which is sensitive to $K\downarrow$ introducing an error which is difficult to quantify [36]. On the modeling side, ENVI-met 3.1 is initialized with a constant cloud cover value which does not always reflect actual conditions, affecting the magnitude of $K\downarrow$. The large midday differences, however, are more likely due to the way ENVI-met calculates *MRT*:

$$MRT = \left[\frac{1}{\sigma_b}\left(E_t(z) + \frac{\alpha_k}{\varepsilon_p}(D_t(z) + I_t(z))\right)\right]^{0.25} \quad (3)$$

where σ_b, α_k and ε_p are the Stefan Boltzmann constant, a body's total absorption coefficient for shortwave radiation (~0.7) and emissivity (~0.97), and $E_t(z)$, $D_t(z)$ and $I_t(z)$ are longwave, total diffuse shortwave and direct shortwave radiation flux absorbed by a body at height z, respectively. The latter is calculated using:

$$I_t(z) = f_p K\downarrow_{dir} \quad (4)$$

where f_p is the proportion of the surface of an upright, rotationally symmetric body that is exposed to direct incoming solar radiation $K\downarrow_{dir}$. f_p changes with time of the day and is estimated according to:

$$f_p = 0.43\cos\gamma + 0.043\sin\gamma \quad (5)$$

The midday dip seen in Fig. 6 follows from lower f_p values around noon when the body is exposed to a smaller amount of $K\downarrow_{dir}$. This characteristic is accentuated under clear conditions when $K\downarrow$ is predominantly composed of direct rather than diffuse radiation.

The calculations are further affected by the fact that ENVI-met uses a particular f_p formulation (Eq. (5)), which differs from the VDI [49] standard conventionally used in biometeorological studies [50]. The largest percentage differences between the two methods are seen at $\gamma = 90°$ (Table 5). MRT has subsequently been recalculated by substituting Eq. (5) with the VDI equation in Eq. (4) and using typical values for $E_t(z)$, $D_t(z)$ and $K\downarrow_{dir}$. *MRT* calculated using the VDI approach shows a much lower afternoon peak value, much reduced midday dip, and generally lower daytime magnitudes (Fig. 7), providing better agreement with the observations. The influence of f_p on the midday dip is likely smaller during very cloudy or overcast conditions when the direct component of the incoming shortwave radiation is reduced.

The larger systematic nighttime errors (Table 3) suggest that further improvements are possible. Since the nighttime radiation exchange is solely due to longwave radiation, the systematic underprediction observed in Fig. 6, which is getting worse as the night progresses, is likely related to an under-prediction of the temperature of the grass surface in the immediate vicinity of R1 (Table 1). Surface moisture seems to have no or little influence given the absence of significant differences between model and observations across seasons (Fig. 6).

5. Impact of urban design on canopy-layer air and mean radiant temperature

To investigate the influence of (i) further urban development and (ii) the implementation of common "UHI mitigation" strategies, ENVI-met is used to simulate changes to T_a and *MRT* for five simulation scenarios (Table 6). The expression "UHI mitigation" is used here, although what is meant is reduction of local canopy-layer temperature without consideration of a "rural" reference. The application of high albedo (i.e. light-coloured) materials is often recommended as an efficient UHI mitigation method through reducing solar heat gains in building envelopes and urban structures [51,52]. Two scenarios therefore examine the impacts of "cool roofs" by increasing α_r (CR), and a more general "high albedo" scenario where the wall albedo is also increased (CR/CW). Emmanuel et al. [13] suggested compact urban forms as a method to mitigate daytime air temperatures in tropical cities through additional shading provided by a combination of tall buildings and narrow roads. The height of buildings shorter than 12 m is therefore doubled in a scenario to investigate the impact of urban density (H2). This almost doubles the average height-to-width ratio (H/W) across the six built-up receptor locations from 0.45 to 0.88, and reflects ongoing urban densification and in-fill found at the present study site and more widely across Singapore. Vegetated roofs are another common UHI mitigation strategy for both arid and humid tropical climates [53–55] which is addressed with a "green roof" scenario, where all rooftops in the model domain are covered with grass (GR). In view of recent and ongoing road-widening projects which have resulted in the loss of large, mature trees providing shade, and new developments in areas previously covered by secondary rain forest, a final scenario removes all trees along streets and in parks (NT). The scenario results are compared against SIM8. This simulation is used as the baseline because, one of good model performance for both T_a and *MRT*, and two it reflects SW-monsoon conditions when T_a and *MRT* are higher contributing to more thermally stressful conditions.

The most drastic temperature reduction is obtained for H2 which has clearly lower daytime T_a between noon and the late afternoon, reaching a maximum reduction of ~0.35 °C at ~16 h (Fig. 8). This is likely due to additional shading provided by walls, an

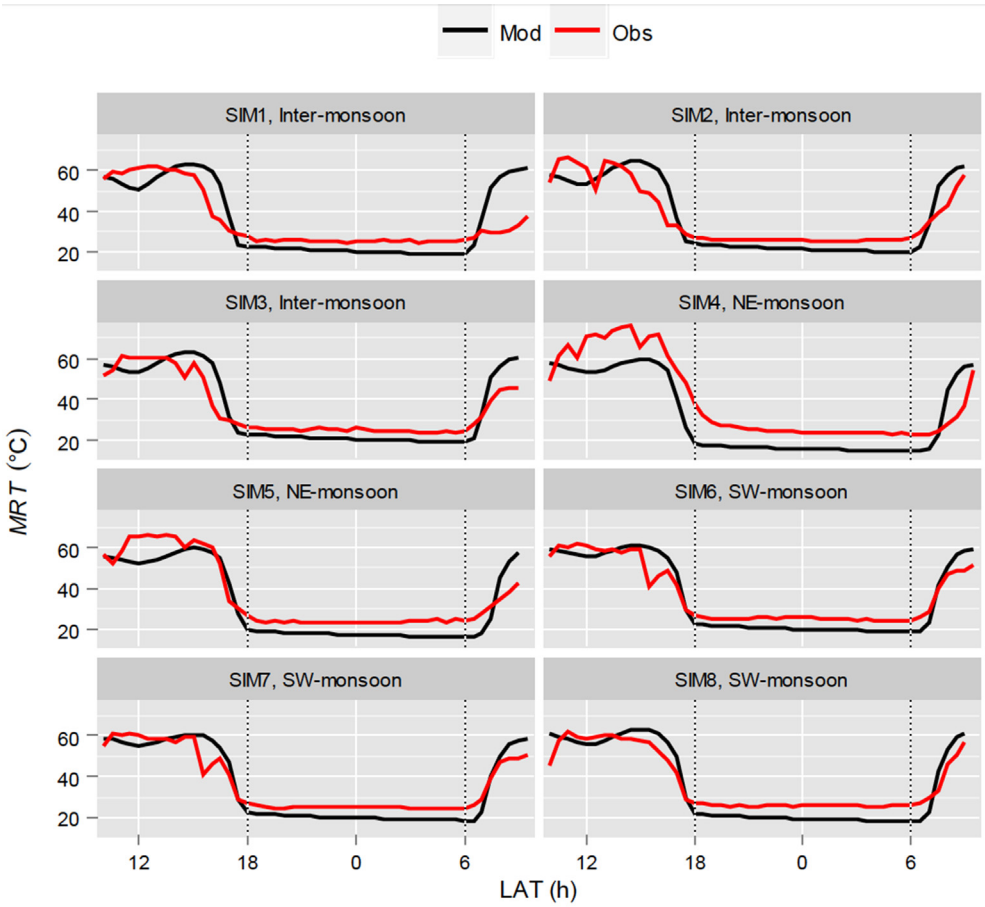

Fig. 6. Comparison between observed (red line) and simulated by ENVI-met (black line) diurnal variability of 1.1-m mean radiant temperature (*MRT*) at R1 for eight days (SIM1 – SIM8) during three seasons. Vertical dotted lines indicate times of sunset and sunrise, respectively. (For interpretation of the references to colour in this figure legend, the reader is referred to the web version of this article.)

Table 4
Change in domain average 2-m air temperature (T_a) simulated by ENVI-met as a result of a change in (top rows) relative soil humidity (*RSH*) and (bottom rows) soil temperature (T_s) in steps of 10% and 1 °C, respectively (across all three soil layers).

RSH						
Change in *RSH* (%)	−30	−20	−10	+10	+20	+30
Resultant change in T_a (°C)	+1.82	+1.39	+0.64	−0.21	−0.23	−0.22
T_s						
Change in soil temperature (°C)	−3	−2	−1	+1	+2	+3
Resultant change in mean T_a (°C)	−0.37	−0.22	−0.09	−0.12	+0.30	+0.50

Table 5
Surface projection factor (f_p) at different solar elevation angles (γ) calculated using ENVI-met ($f_{p\text{-}ENVI}$) (Eq. (5)) and VDI [49] ($f_{p\text{-}VDI}$), respectively.

γ (°)	10	20	30	40	50	60	70	80	90
$f_{p\text{-}ENVI}$	0.42	0.41	0.39	0.35	0.30	0.25	0.18	0.12	0.04
$f_{p\text{-}VDI}$	0.31	0.28	0.25	0.23	0.20	0.17	0.14	0.12	0.09

effect which is more pronounced if $\boldsymbol{z_h}$ of all buildings is further increased to 25 m ($H/W = 1.32$) and late afternoon temperatures are reduced by 0.7 °C (not shown). The model further suggests a cooling effect that diminishes throughout the night. This is surprising given the expectation of reduced longwave radiation loss due to higher built density as one of the main factors contributing to higher canopy-layer temperatures. This result, however, is likely also due to the model not considering heat storage in buildings.

The second most significant daytime temperature reduction is observed for CR, with a cooling of ~0.25 °C at around noon, or 0.45 °C if α_r is increased to 0.8 (not shown). Simultaneously reducing α_w decreases the mitigation effect by about half and even results in warming compared to the baseline in the late afternoon, possibly due to increased multiple reflections of shortwave radiation off the bright walls. T_a subsequently remains higher than the baseline at the beginning of the night and decreases slowly towards sunrise. As expected, increasing α_r alone has no effect on nighttime T_a. The GR scenario results in the least daytime T_a reduction (~0.1 °C), but rooftop vegetation retains a cooling influence throughout the night (up to 0.14 °C). The real mitigation effect of GR, however, may be underestimated because ENVI-met does not support the implementation of soil on vegetated roofs and

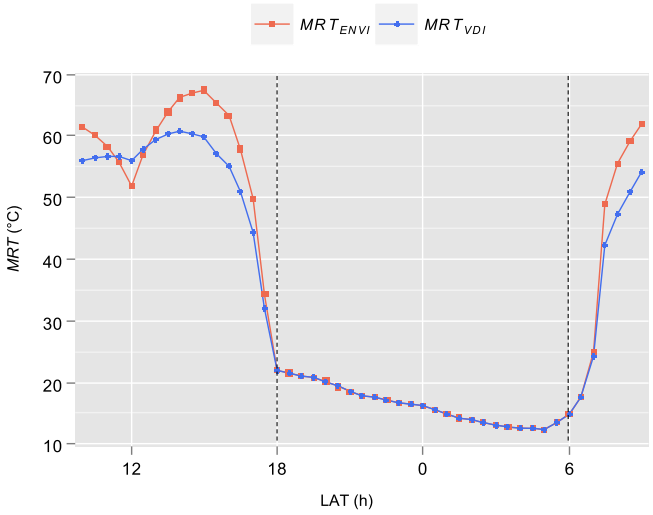

Fig. 7. Diurnal variability of 1.1-m mean radiant temperature (*MRT*) at R1 calculated using ENVI-met default Eq. (4) (MRT_{ENVI}) and VDI [49] (MRT_{VDI}), respectively. Vertical dotted lines indicate times of sunset and sunrise, respectively.

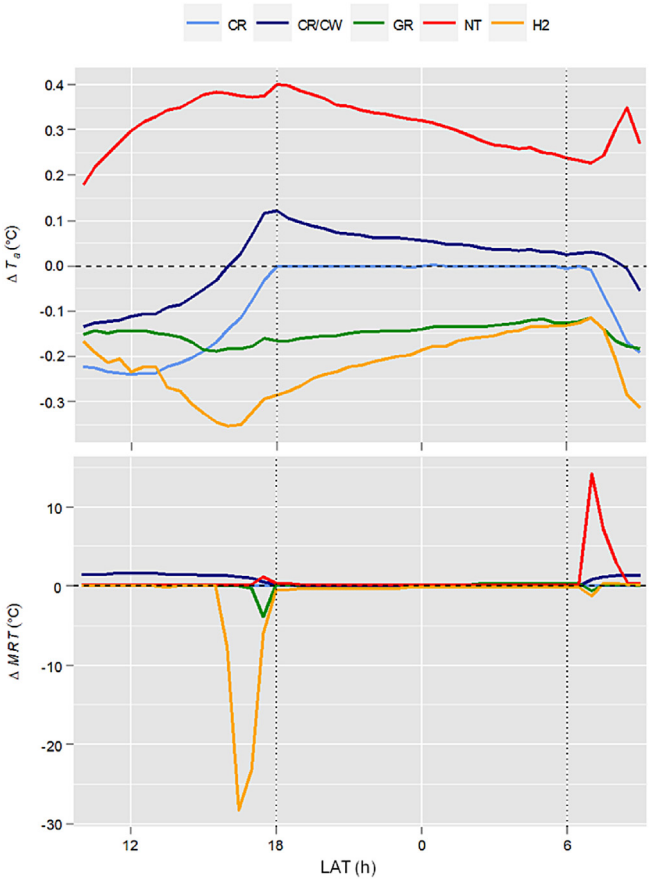

Fig. 8. Diurnal variability of difference between five simulation scenarios (CR, CR/CW, GR, NT and H2) and a baseline (SIM8) for (top) domain average 2-m air temperature and (bottom) 1.1-m mean radiant temperature at R1. Vertical dotted lines indicate times of sunset and sunrise, respectively.

therefore neglects the possible influence of rooftop soil moisture on T_a. Unlike for CR, GR has the potential to provide cooling not just during day- but nighttime as well. Removing trees (NT) significantly increases daytime T_a (~0.2–0.4 °C), which remains above the baseline throughout the night.

The impact of the various scenarios on *MRT* is limited to daytime given its dependence on $K\downarrow_{dir}$ (Fig. 8). H2 (NT) results in the greatest *MRT* reduction (increase), which is most pronounced in the late afternoon (early morning) reaching −28 (~14) °C. The temporal asymmetry around noon is attributed to the sun-obstacle geometry, and the extent to which taller buildings and trees at R1 provide shade. This suggests that properly considering the orientation of buildings or location of trees can reduce heat stress and greatly affect OTC. As expected, modifying roof characteristics such as in scenarios CR and GR has little influence on street-level *MRT*. CR/CW, however, shows that an additional increase in α_w results in slightly higher daytime *MRT* compared to the baseline since additional reflection off high-albedo walls increases the radiant fluxes the body is exposed to. Similar results have been observed in Colombo, Sri Lanka [13] and Melbourne, Australia [20]. The discussion above applies to *MRT* and hence radiation, and neglects wind which is another important component of thermal stress. Some of the beneficial benefits noted due to shading may be partially offset by lower wind speed which would be present in e.g. deeper street canyons such as in scenario H2.

6. Summary and conclusions

The present study evaluates the performance of an urban microclimate model (ENVI-met 3.1) to predict canopy-layer T_a and *MRT* over a residential neighbourhood of a tropical city, viz. Singapore. Measurements at seven locations during eight, mostly clear and calm days representing three different seasons with dry and wet surface conditions, constitute the evaluation dataset. Detailed initialization data (e.g. soil relative humidity, leaf area density profile) are obtained to accurately represent the local conditions. The diurnal course of T_a is predicted well across all days considered, with the timing of the daytime maximum and nighttime minimum T_a within ±2 h of the respective observations. Absolute magnitudes are simulated more accurately during the wet compared to dry seasons as reflected by the daily model evaluation metrics. Systematic differences prevail and are particularly pronounced during dry conditions when the model overestimates T_a from early afternoon throughout nighttime until close to sunrise. This result is likely due to limitations in the soil model when *RSH* is low. The model is also able to differentiate individual sites within

Table 6
Five mitigation/land cover change scenarios and associated changes in urban design variables compared to a baseline (SIM8). α_r, α_w, z_h — albedo of roofs, walls and mean building height, respectively; nc — no change compared to Baseline scenario.

Scenario (Code)	α_r	α_w	Vegetation (%)	z_h (m)
Baseline	0.16	0.25	8.1% shade tress along streets and in parks	10.6
Cool roof (CR)	0.50	nc	nc	nc
High albedo (CR/CW)	0.50	0.50	nc	nc
Selective doubling of building height (H2)	nc	nc	nc	2× z_h if original height is <12
Green roofs (GR)	nc	nc	Grass-covered roofs on all buildings (39.8% plan area)	nc
No trees (NT)	nc	nc	Removal of 8.1% shade trees along streets and in parks	nc

the modeling domain, accurately predicting maximum day- and nighttime differences between the built-up sites and the park location. Despite some inter-seasonal variability, the present results suggest better model performance compared to similar studies conducted elsewhere. RMSE magnitudes are smaller than those reported by Ref. [12] (2.61–2.73 and 1.06–2.80 °C for day- and nighttime, respectively) [21], (2.96 °C) [22], (2.79–3.60 °C), or [24] (1.41–2.00 °C). One reason suggested for the better performance is the more accurate representation of model input variables in the present study.

In the case of *MRT*, the model is able to predict the magnitude of the daytime maximum, but it systematically underpredicts nighttime values with little dependence on season. Modelled *MRT*, however, displays a pronounced double daytime peak with the minimum centered on noon which is not present in the observations. This feature is suggested to follow from the way the model calculates *MRT*, and largely disappears if an alternative equation for the projection factor in the calculation of the direct shortwave radiation flux absorbed by a body is used. Nevertheless, given the ability to simulate daytime *MRT* maxima, the model offers the opportunity to assess daytime extremes in thermal comfort conditions.

With proper model initialization and awareness of its limitations, the present study shows that ENVI-met is a helpful tool for simulating the main features of the diurnal variability of T_a and *MRT*. The model has therefore been used to investigate five temperature mitigation or land cover change scenarios. The largest daytime reduction (up to ~0.35 °C) is observed from doubling building heights, which also results in the largest reduction of *MRT* (up to ~28 °C), which are both due to increased shading from increased *H/W*. The model also calculates a nighttime reduction in T_a, however, there is less confidence in this result, given the model's inability to account for heat storage in buildings. While increasing α_r produces a similar reduction in daytime T_a (~0.24 °C) compared to that observed from doubling building heights, nighttime T_a remains unaffected. Increasing both α_r and α_w partially offsets the daytime cooling effects from increased α_r, but increases T_a at night, and notably daytime *MRT* due to increased shortwave radiation reflected off the brighter walls. Green roofs reduce T_a throughout the day, but the effect is less (~0.1 °C) compared to the previous two options. Removing all trees significantly increases daytime T_a (by up to 0.4 °C) and *MRT* (~14 °C). In the end, the relative effectiveness of the various scenarios is difficult to assess, and in part depends on the magnitude of changes suggested for the various control variables. The non-uniformity of impacts also highlights the microclimatic and bioclimatic complexities inherent in a heterogeneous urban system. Further, while increasing building heights may seem a relatively efficient option to reduce daytime T_a, increasing building density will increase drag, reduce canopy-layer wind and the dispersive capability of the local atmosphere and potentially give raise to air quality issues.

The release of the latest version of ENVI-met 4.0 [30] addresses some of the issues mentioned above. It includes changes to how the heat transfer between the interior of buildings, building walls and the surrounding environment is calculated, which should provide some form of building heat storage and hence improve nighttime predictions of temperature. The new version also provides the ability to prescribe the diurnal variation of meteorologically relevant boundary conditions. The soil model, however, has not been altered in ENVI-met 4.0 and the issues related to *RSH* pointed out above and the proper characterization of the surface wetness remain. The present work further illustrates how the choice of the f_p equation used contributes to the particular daytime shape of *MRT* variability, and suggests an alternative method which agrees better with observations. Finally, while it is easier to evaluate state variables, a thorough evaluation should also investigate the sensible and latent heat fluxes. This will illuminate the specific sources of model error in other dependent variables like air and surface temperature or humidity, which all are important components of thermal comfort and heat stress indices.

Acknowledgements

This research was supported by a National University of Singapore (grant numbers R-109-000-091-112, R-109-000-185-112). The authors thank S.H. Tan, S. Harshan and E. Velasco for their assistance in the field, and M. Cher (East Lodge Hostel) for access to the measurement site.

References

[1] T.R. Oke, The energetic basis of the urban heat island, Quat. J. R. Meterol. Soc. 108 (455) (1982) 1–24.
[2] A.J. Arnfield, Two decades of urban climate research: a review of turbulence, exchanges of energy and water, and the urban heat island, Int. J. Climatol. 23 (1) (2003) 1–26.
[3] R. de Dear, Human thermal climate of Singapore, Singap. J. Trop. Geogr. 10 (1) (1989) 13–26.
[4] E.M. Fischer, K.W. Oleson, D.M. Lawrence, Contrasting urban and rural heat stress responses to climate change, Geophys Res. Lett. 39 (2012) L03705.
[5] M. Roth, Review of urban climate research in (sub)tropical regions, Int. J. Climatol. 27 (2007) 1859–1873.
[6] M. Roth, W.T.L. Chow, A historical review and assessment of urban heat island research in Singapore, Singap J. Trop. Geogr. 33 (2012) 381–397.
[7] J.K.S. Ching, A perspective on urban canopy layer modeling for weather, climate and air quality applications, Urban Clim. 3 (2013) 13–39.
[8] A. Matzarakis, F. Rutz, H. Mayer, Modelling radiation fluxes in simple and complex environments - application of the RayMan Model, Int. J. Biometeorol. 51 (2007) 323–334.
[9] F. Lindberg, B. Holmer, S. Thorsson, SOLWEIG 1.0-Modelling spatial variations of 3D radiant fluxes and mean radiant temperature in complex urban settings, Int. J. Biometeorol. 52 (2008) 697–713.
[10] A. Matzarakis, O. Matuschek, Sky view factor as a parameter in applied climatology – rapid estimation by the Sky Helio model, Meteorol. Z. 20 (1) (2011) 39–45.
[11] M. Bruse, H. Fleer, Simulating surface-plant-air interactions inside urban environments with a three dimensional numerical model, Environ. Modell. Softw. 13 (1998) 373–384.
[12] R. Emmanuel, H.J.S. Fernando, Urban heat islands in humid and arid climates: role of urban form and thermal properties in Colombo, Sri Lanka and Phoenix, USA, Clim. Res. 34 (2007) 241–251.
[13] R. Emmanuel, H. Rosenlund, E. Johansson, Urban shading - a design option for the tropics. A study in Colombo, Sri Lanka, Int. J. Climatol. 27 (2007) 1995–2004.
[14] A.N. Kakon, N. Mishima, S. Kojima, Simulation of the urban thermal comfort in a high density tropical city: analysis of the proposed urban construction rules for Dhaka, Bangladesh, Build. Simul. 291–305 (2009) 2.
[15] F. Yang, S.S.Y. Lau, F. Qian, Thermal comfort effects of urban design strategies in high-rise urban environments in a sub-tropical climate, Archit. Sci. Rev. 54 (2011) 285–304.
[16] E. Ng, L. Chen, Y. Wang, C. Yuan, A study on the cooling effects of greening in a high-density city: an experience from Hong Kong, Build. Environ. 47 (2012) 256–271.
[17] A. Qaid, D.R. Ossen, Effect of asymmetrical street aspect ratios on microclimates in hot, humid regions, Int. J. Biometeorol. 59 (2015) 657–677.
[18] F. Ali-Toudert, H. Mayer, Numerical study on the effects of aspect ratio and orientation of an urban street canyon on outdoor thermal comfort in hot and dry climate, Build. Environ. 41 (2006) 94–108.
[19] F. Ali-Toudert, H. Mayer, Effects of asymmetry, galleries, overhanging facades and vegetation on thermal comfort in urban street canyons, Sol. Energy 81 (2007) 742–754.
[20] N.M.J. d'Argent, A Microclimatic and Bioclimatic Assessment of the Compact City Morphology: a Case Study of Melbourne @ 5 Million (Ph.D. thesis), Monash University, Melbourne, Australia, 2012.
[21] W.T.L. Chow, R.L. Pope, C.A. Martin, A.J. Brazel, Observing and modeling the nocturnal park cool island of an arid city: horizontal and vertical impacts, Theor. Appl. Climatol. 103 (2011) 197–211.
[22] W.T.L. Chow, A.J. Brazel, Assessing xeriscaping as a sustainable heat island mitigation approach for a desert city, Build. Environ. 47 (2012) 170–181.
[23] J. Declet-Barreto, A.J. Brazel, C.A. Martin, W.T.L. Chow, S.L. Harlan, Creating the park cool island in an inner-city neighborhood: heat mitigation strategy for Phoenix, AZ, Urban Ecosyst. 16 (3) (2013) 617–635.
[24] A. Middel, K. Häb, A.J. Brazel, C.A. Martin, S. Guhathakurta, Impact of urban form and design on mid-afternoon microclimate in Phoenix Local Climate Zones, Landsc. Urban Plan. 122 (2014) 16–28.

[25] B.C. Hedquist, A. Brazel, Seasonal variability of temperatures and outdoor human comfort in Phoenix, Arizona, U.S.A, Build. Environ. 72 (2014) 377–388.
[26] G. Maggioto, R. Buccolieri, M.A. Santo, L.S. Leo, S. di Sabatino, Validation of temperature-perturbation and CFD-based modelling for prediction of the thermal environment. The Lecce (IT) case study, Environ. Model. Softw. 60 (2014) 69–83.
[27] F. Salata, I. Golasi, R. de Lieti Vollaro, A. de Lieto Vollaro, Urban microclimate and outdoor thermal comfort. A proper procedure to fit ENVI-met simulation outputs to experimental data, Sustain. Cities Soc. 26 (2016) 318–343.
[28] X.S. Yang, L.H. Zhao, M. Bruse, Q.L. Meng, Evaluation of a microclimate model for predicting the thermal behavior of different ground surfaces, Build. Environ. 60 (2013) 93–104.
[29] N. Oreskes, Role of quantitative models in science, in: C.D. Canham, J. Cole, W.K. Lauenroth (Eds.), Models in Ecosystem Science, Princeton University Press, Princeton, 2003, pp. 13–31.
[30] ENVI-met, 2015. http://www.envi-met.com (accessed 5 June 2015).
[31] W.T.L. Chow, M. Roth, Temporal dynamics of the urban heat island of Singapore, Int. J. Climatol. 26 (2006) 2243–2260.
[32] W.T.L. Chow, Siti Nur 'Assyakirin Binte Ali Akbar, L.H. Su, M. Roth, Assessment of measured and perceived microclimates within a tropical urban forest, Urban For. Urban Green. 16 (2016) 62–75.
[33] I.D. Stewart, T.R. Oke, Local Climate Zones for urban temperature studies, Bull. Am. Meteorol. Soc. 93 (2012) 1879–1900.
[34] E. Velasco, M. Roth, S.H. Tan, M. Quak, S.D.A. Nabarro, L. Norford, The role of vegetation in the CO_2 flux from a tropical urban neighbourhood, Atmos. Chem. Phys. 13 (2013) 10185–10202.
[35] M. Roth, C. Jansson, E. Velasco, Multi-year energy balance and carbon dioxide fluxes over a residential neighborhood in a tropical city, Int. J. Climatol. (2016), http://dx.doi.org/10.1002/joc.4873, 20 pages.
[36] S. Thorsson, F. Lindberg, I. Eliasson, B. Holmer, Different methods for estimating the mean radiant in an outdoor urban setting, Int. J. Climatol. 27 (2007) 1983–1993.
[37] ASHRAE, Handbook of Fundamentals. American Society of Heating, Refrigerating and Air-conditioning Engineers, 1997.
[38] C.L. Tan, N.H. Wong, S.K. Jusuf, Outdoor mean radiant temperature estimation in the tropical urban environment, Build. Environ. 64 (2013) 118–129.
[39] G.L. Mellor, T. Yamada, A simulation of the Wangara atmospheric boundary layer data, J. Atmos. Sci. 32 (1975) 2309–2329.
[40] OneMap, 2013. http://www.onemap.sg (accessed 5 June 2015).
[41] BCA, Code for Environmental Sustainability of Buildings Version 1.0. Building Codes, Building and Construction Authority, Singapore, 2008.
[42] T.R. Oke, Inadvertent climate modification, in: Boundary Layer Climates, second ed., Methuen, London, U.K., 1987, pp. 262–303.
[43] B. Lalic, D.T. Mihailovic, An empirical relation describing leaf-area density inside the forest for environmental modelling, J. Appl. Meteorol. 43 (2004) 641–645.
[44] P.Y. Tan, S. Angelia, Leaf Area Index of Tropical Plants:A Guidebook on its Use in the Calculation of Green Plot Ratio, National Parks Board, Singapore, 2010.
[45] M.R. Gale, D.F. Grigal, Vertical root distributions of northern tree species in relation to successional status, Can. J. For. Res. 17 (8) (1987) 829–834.
[46] R.B. Jackson, J. Canadell, J.R. Ehleringer, H.A. Mooney, O.E. Sala, E.D. Schulze, A global analysis of root distributions for terrestrial biomes, Oecologia 108 (1996) 389–411.
[47] C.J. Willmott, Some comments on the evaluation of model performance, Bull. Am. Meteorol. Soc. 63 (11) (1982) 1309–1313.
[48] C.J. Willmott, On the validation of models, Phys. Geogr. 2 (1981) 184–194.
[49] VDI, Methods for the Human-biometeorological Assessment of Climate and Air Quality for Urban and Regional Planning, in: Part 1: Climate. VDI Guideline 3787, VDI, Berlin, 1998.
[50] F. Ali-Toudert, Dependence of Outdoor Thermal Comfort on Street Design in Hot and Arid Climate (Ph.D. thesis), University of Freiburg, Germany, 2005.
[51] A.H. Rosenfeld, H. Akbari, S. Bretz, B.L. Fishman, D.M. Kurn, D. Sailor, H. Taha, Mitigation of urban heat islands: materials, utility programs, updates, Energy Build. 22 (1995) 255–265.
[52] S. Santamouris, Cooling the cities – a review of reflective and green roof mitigation technologies to fight heat island and improve comfort in urban environments, Sol. Energy 103 (2014) 682–703.
[53] A. Akbari, M. Pomerantz, H. Taha, Cool surfaces and shade trees to reduce energy use and improve air quality in urban areas, Sol. Energy 70 (3) (2001) 295–310.
[54] L. Shashua-Bar, M.E. Hoffman, Quantitative evaluation of passive cooling of the UCL microclimate in hot regions in summer, case study: urban streets and courtyards with trees, Build. Environ. 39 (2004) 1087–1099.
[55] E. Alexandri, P. Jones, Temperature decreases in an urban canyon due to green walls and green roofs in diverse climates, Build. Environ. 43 (2008) 480–493.